Vol 104, No. 1039

Life extending control of aircraft: trade-off between flight performance and structural durability

A. Ray and J. Caplin
Pennsylvania State University, USA

ABSTRACT

The goal of life extending control (LEC) is to enhance the service life of complex mechanical systems, such as aircraft, spacecraft, and energy conversion devices, without any significant loss of performance, and can be achieved by making a trade-off between dynamic performance and structural durability. This paper presents the concept and a design methodology for robust life extending control of aircraft structures that are typically subjected to cyclic mechanical stresses. The controller design procedure relies on the specifications of flight performance and allowable fatigue crack damage at critical points of aircraft structures that serve as indicators of the effective service life. As an example, an aeroelastic model of the aircraft wings has been formulated and is incorporated into a nonlinear rigid-body model of the flight-dynamics. The H_∞–based structured singular value (μ) synthesis method has been used to design robust life extending controllers based on a linearised model of the aircraft and a (nonlinear) state-space model of fatigue crack growth. The results of simulation experiments show significant savings in fatigue life of the wings while retaining the dynamic performance of the aircraft.

1.0 INTRODUCTION

In the post-Cold War era, there is an increasing concern about high acquisition and maintenance cost associated with complex weapons systems. Fighter aircraft are a good example of such systems because the airframe undergoes significant cyclic stresses resulting in the need for frequent inspection and replacement of critical components. While airframe manufacturers are constantly updating the technology base to handle higher stress levels, these improvements often do not fully translate into an equivalent increase in component life due to the ever-increasing performance requirements of fighter aircraft. This is particularly true of the current generation of fighter aircraft, as the high thrust-to-weight ratio allows extreme flight manoeuvres that were not possible earlier and thereby the airframe is often subjected to very high instantaneous and sustained stress levels.

From an economic standpoint it is desirable to obtain the maximum amount of useful life from the most expensive (and hard to replace) components of the aircraft, as well as to reduce the number of maintenance inspections required to ensure structural integrity of critical components. This practice is also desirable from an operational viewpoint, since reductions in downtime for inspection and repair result in increased availability. However, since failure of certain components may result in loss of the aircraft, and more importantly, loss of human life, safety considerations mandate replacement of all critical components before a failure is likely to occur. This requirement is realised in the following way. A fighter aircraft that exceeds its design load factor during a flight is temporarily removed from service, and it must undergo a rigorous inspection to determine if any special maintenance is required prior to its return to flying status. (Note: Load factor is defined as the total lift force acting on the aircraft divided by the aircraft weight).

Designers of flight control systems have recognised the possibility of actively reducing damage in certain aircraft structures, particularly the wing. The simplest concept that is currently employed on both F-16 and F/A-18 aircraft is the so-called 'g-limiter'. It serves to limit the aircraft's maximum load factor to a predefined value. Transport aircraft have used the gust load alleviation (GLA) system[1,2] that uses feedback from accelerometers on the wing to drive special control surfaces in order to reduce the additional loads imposed by atmospheric disturbances. A similar concept, known as manoeuvre load alleviation (MLA)[3] or manoeuvre load control (MLC)[4], has been proposed for high-performance aircraft. The aim of these systems is to shift the lift distribution inboard during high loading conditions to limit the bending moment at the wing root. Dynamic stresses have been considered in the so-called fatigue reduction (FR) system[3] that seeks to minimise the amplitude and/or number of stress cycles experienced at the critical point(s). While these systems have shown tangible benefits, there is apparently a common weakness that may well prevent them from achieving their maximum potential. In all cases, the actual dynamics of the fatigue crack damage phenomenon in the structural material are not included in the analysis. It is simply assumed that, by limiting the peak stress at the critical points of the structure, life-savings are maximised. Since stress overloads could result in transient retardation of crack growth[5,6], the frequency content of the applied stresses could be shaped by control actions to achieve larger fatigue life than the traditional approach of simply limiting the peak stress.

This paper addresses the above issue focusing on fatigue damage

Paper No. 2556. Manuscript received 4 May 2000, accepted 31 July 2000.
The research work reported in this paper has been supported in part by National Science Foundation under Grant No CMS-9819074; National Academy of Sciences under a Research Fellowship award to the first author.

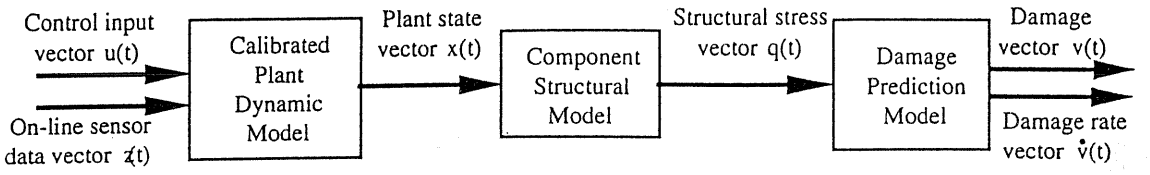

(a) Generic Damage Prediction System

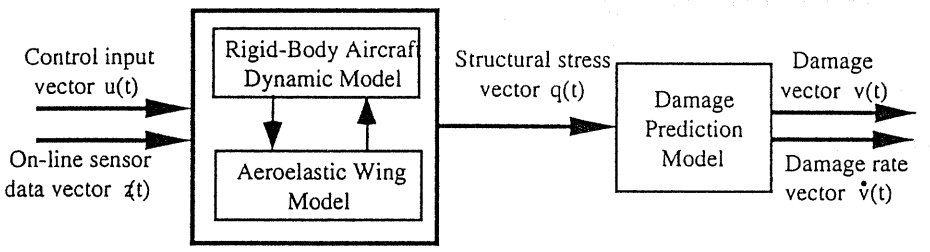

(b) Aircraft Wing Damage Prediction System

Figure 1. Schemes for on-line damage prediction.

mitigation in the wings of high performance aircraft that are usually instrumented for health monitoring and control. The life extension feature of the control system can be activated or deactivated at the pilot's discretion. The thrust of the paper is on robust life extending control (LEC) where the goal is to achieve large gains in structural durability by manipulation of stress profiles with no significant loss of performance[7]. This concept of LEC has been investigated for reusable rocket engines[8,9], rotorcraft[10], and fossil fuel power plants[11,12]. In all cases, simulation results show a substantial increase in component life with no significant loss in system performance. Efficacy of the LEC concept has also been demonstrated by laboratory experimentation on a test apparatus[13]. The design approach presented in this paper is different from the previously reported work in the following sense:

- Ranges in aerodynamic forces due to structural deformation have been included in the plant dynamic model in combination with the rigid body model.
- There is no need for an optimal feedforward control sequence that suffers from sensitivity to plant modelling uncertainties as well as from variations in the initial conditions.

The paper is organised in five sections including the introduction. Section 2 describes model formulation for life extending controller design. Section 3 presents a procedure for synthesis of the robust life-extending control law. Section 4 presents the overall structure of life extending control simulation and the results of the aircraft performance and crack-growth damage for a family of robust controllers. Section 5 summarises and concludes the paper with recommendations for future work.

2.0 MODEL FORMULATION FOR LIFE EXTENDING CONTROLLER DESIGN

Although controller design for highly flexible aircraft, such as transports, requires dynamic models that explicitly include structural flexibility[3], these effects are often ignored on aircraft that experience relatively small elastic deformation. This is particularly true when modern robust control techniques, such as H_∞–synthesis, are employed, since the effects of unmodelled dynamics due to flexibility can be included within the (unstructured) uncertainty model. However, explicit modelling of structural flexibility may provide a solution to another problem faced by flight control systems designers, namely that of control surface redundancy. High-performance aircraft require two (or more) different sets of control surfaces for roll control and, in some cases, have multiple controls for pitch and yaw as well. As these controls have different levels of effectiveness at different flight conditions, they appear to be redundant actuators in the controller synthesis process at a given operating condition. Therefore, special measures are required to allocate commands between the various control surfaces. Methods that have been developed to date include the use of a nonlinear control selector[14], or the use of off-line constrained optimisation procedures[15]. In both cases, the methods only examine the effects of the controls on the rigid-body motion of the aircraft.

The life extending control (LEC) takes advantage of the control surface redundancy by utilising the elastic behaviour of the aircraft structure as well as the rigid-body motion. The theme of LEC design is that different locations of control surfaces on the airframe may result in different effects on the elastic modes of the aircraft structure. Thus, the control systems designer can make use of all available control surfaces to simultaneously achieve the desired level of performance while mitigating the structural damage by reshaping the stress profile. So far the only application of LEC to aviation systems has been the work of Rozak and Ray[10,16] who developed a H_∞–based robust controller for rotorcraft with the objective of reducing damage to the control horn of the main rotor. Since the control horn does not directly experience any significant aerodynamic forces, the loading is of a purely mechanical nature, and hence the analysis fits very well into the framework depicted in Fig. 1(a). In contrast, the loads (and hence stresses) acting on an aircraft wing occur due to aeroelasticity, which deals with interactions of aerodynamic forces with flexible structures. Since the aerodynamic loading depends on the body geometry, and the geometry in turn depends on the loading, it is not possible to determine the loading and deformation independently. The aerodynamic forces play a dominant role in determining the dynamics of the aircraft that, in turn, lead to deformations and stresses in the critical structures. Hence, the aeroelastic model of aircraft wing is absorbed into the plant dynamic model to capture the changes in aerodynamic forces due to the wing deformation as shown in Fig. 1(b).

Control surface	Transfer Function	Deflection limits (deg)	Rate (deg/sec)
Aileron	$\frac{1\cdot0}{\left(\frac{s}{75\cdot0}\right)^2\left(\frac{2\times0\cdot59}{75\cdot0}\right)s+1\cdot0}$	±20	±100
Rudder	$\frac{1\cdot0}{\left(\frac{s}{72\cdot0}\right)^2\left(\frac{2\times0\cdot69}{72\cdot0}\right)s+1\cdot0}$	±30	±100
Stabilator	$\frac{\left(\frac{s}{82\cdot9}\right)^2\left(\frac{2\times0\cdot068}{82\cdot9}\right)s+1\cdot0}{\left[\left(\frac{s}{36\cdot4}\right)^2\left(\frac{2\times0\cdot41}{36\cdot4}\right)s+1\cdot0\right]\left[\left(\frac{s}{105\cdot3}\right)^2\left(\frac{2\times0\cdot59}{105\cdot3}\right)s+1\cdot0\right]}$	+15/−25	±60

Table 1
Dynamic models of actuators

2.1 The rigid body model

The rigid-body flight dynamic model in this paper is similar to the corresponding model developed for the AIAA Controls Design Challenge[17]. Therefore, the governing equations of the rigid body model are not repeated here. The control surfaces include left and right ailerons, left and right stabilators, and a single rudder. Although the aircraft has five control surfaces, only four variables are required to specify their positions: the aileron deflection δ_A; the rudder deflection δ_R , the symmetric stabilator deflection δ_H; and the differential stabilator deflection δ_D. The positions of the individual control surfaces are determined as follows:

left aileron position = $0{\cdot}5\delta_A$; *right aileron position* = $-0{\cdot}5\delta_A$ *left stabilator position* = $\delta_H + 0{\cdot}5\delta_D$; *right stabilator position* = $\delta_H - 0{\cdot}5\delta_D$ *rudder position* = δ_R

In the original model of Brumbaugh[17], all actuator dynamics are represented as first order lags with a time constant of 50ms that has been replaced with more detailed dynamics[18]. The transfer functions and rate limits of the actuators are given in Table 1.

Linearisation of the equations of motion for a rigid, fixed-wing aircraft yields two uncoupled sets of equations. One set governs the longitudinal dynamics of the aircraft while the other governs the lateral dynamics. We have followed the standard practice to design separate controllers for lateral and longitudinal dynamics based on the uncoupled linearised models and then evaluate the control system based on the simulation of the nonlinear model.

The stick-fixed longitudinal motion of a rigid aircraft disturbed from an equilibrium flight condition is described by two oscillatory modes of motion: the short period mode and the long period (or phugoid) mode. The short period mode typically has a period on the order of a few seconds, with motion characterised by changes in angle-of-attack, pitch angle, and altitude, while the flight velocity remains practically constant. The phugoid mode has a much longer period, on the order of tens or hundreds of seconds, with motion characterised by changes in velocity, pitch angle, and altitude, with angle-of-attack remaining approximately constant. Because of the slow dynamics associated with the phugoid mode, this mode has been ignored during the synthesis of the life-extending control laws for manual flight. The pitch rate q and angle-of-attack α are the state variables of interest for longitudinal rigid-body motion. However, for the design of an autopilot (that is not addressed in this paper), the phugoid motion becomes the primary mode of interest.

The desired short period response of the aircraft is that of a second order system. The natural frequency is a function of the acceleration sensitivity of the aircraft, which is the change in load factor per unit change in angle-of-attack. The acceleration sensitivity is determined by the aerodynamics of the aircraft and the particular flight condition under consideration. Thus, the desired natural frequency also varies with different flight conditions. The damping ratio of the short period mode is required to be between 0·35 and 1·3 for all flight conditions based on MIL-F-8785C specifications[19].

The roll rate p, yaw rate r, and sideslip angle β are the state variables of interest for lateral rigid body motion. The stick-fixed lateral motion of a rigid aircraft is described by three natural modes: (*i*) the Dutch roll mode consisting of lightly damped, oscillatory, out-of-phase roll, yaw, and sideslip motions; (*ii*) the roll mode consisting of a non-oscillatory, highly convergent mode describing the rolling characteristics of the aircraft; and (*iii*) the spiral mode consisting of non-oscillatory, convergent or divergent motion following a sideslip disturbance. Note that an unstable spiral mode will cause the aircraft to go into a turn that becomes increasingly tighter with time. The handling qualities requirements specify that the Dutch roll mode should have a frequency of at least 1 radian per second. The damping ratio must be greater than or equal to 0·4, or the product of the frequency and damping ratio should be greater than or equal to 0·4 radians per second, whichever results in the larger value for the required damping. The roll mode requirement states that the roll time constant must be less than or equal to 1·0 second. This requirement is actually conservative with regards to modern fighters, which typically have roll time constants in the range of 0·33 to 0·5 seconds[18]. The spiral mode requirement specifies that the minimum time to reach a 40° bank angle following a bank angle disturbance must be greater than or equal to 12 seconds. Because of the slower dynamics of the spiral mode, it is typically ignored during controller synthesis.

2.2 Atmospheric model

Atmospheric properties are based on the US Standard Atmosphere[20]. The model outputs values for temperature, static pressure, density, and speed of sound as functions of altitude. While not strictly an atmospheric property, the model also includes tabulated values for the acceleration due to gravity, also as a function of altitude. The atmospheric model in this paper is similar to the corresponding model developed for the AIAA Controls Design Challenge[17] and is not repeated here.

2.3 Aeroelastic model

Aerodynamic forces acting on a body depend on the time history of the body's motion[21]. When the dynamics of a rigid aircraft are the subject of interest, particularly if the aircraft does not perform any severe manoeuvres, the much faster dynamics of the flow field are ignored based on the principle of singular perturbation. For aircraft that are required to perform extreme manoeuvres, it is often sufficient to introduce approximate correction factors into the equations of motion to account for any unsteady aerodynamic forces. These correction factors generally depend on the time derivatives of angle-of-attack α and sideslip angle β. However, when the flexible structures of aircraft (that have a faster time scale than the rigid-body dynamics) are of interest, it becomes necessary to explicitly model the dynamics of the flow-field to identify any potential instability due to fluid-structure interactions, known as flutter. Since wing flutter results in catastrophic failure of the aircraft, it is prevented either through the design of the wing, or through the use of active flutter suppression (AFS). Therefore, an aeroelastic model of the critical structure (i.e., the wings) is required for the LEC design for the following reasons:

- To shape the profiles of transient stresses for fatigue damage reduction; and
- To ensure that the control system does not adversely affect the flutter characteristics.

2.4 Structural model

Although composite wing structures have been used in recent aircraft, most fighter aircraft have wings that are at least partially, and in most cases solely, built from ductile alloys. A typical wing structure contains at least two spars that run the length of the wing semi-span to bear the majority of the bending loads. The spars and the skin together form several torsion boxes to resist twisting deformation of the wings. The wings also contain many lesser structural members whose primary function is to maintain the shape of the skin. In this paper, the structural model is formulated as a pair of Euler beams to represent the important structural behaviour of the wings. Each beam model is aligned with the elastic axis (i.e. the line through which loads applied normal to the plane of the wing result in pure bending). The centre portion of the model, where the beams meet, is assigned proportionately higher values of bending and torsional stiffness in order to represent the fuselage. The model is spatially discretised and cast in the finite element setting. While the details of the finite-element model, including the element type and shape functions, are reported by Caplin[22], its basic features and dominant mode shapes are presented below:

The generalised displacement vector $\xi(t)$ is obtained by orthogonal transformation of the physical displacement vector $\theta(t)$, i.e., $\xi(t) = \Phi^T\theta(t)$ where Φ is the orthogonal matrix whose columns are the individual mode shapes. The governing equation for $\xi(t)$ is obtained in the transformed coordinates as:

$$M\ddot{\xi}(t)+C\dot{\xi}(t)+K\xi(t)=f(t) \qquad \ldots(1)$$

where the transformed 'modal mass' and 'modal stiffness' matrices, M and K, are diagonal; C is the 'modal damping' matrix representing energy dissipation; and $f(t)$ the total generalised force vector which is obtained by orthogonal transformation of the applied nodal force vector that is a linear combination of aerodynamic force due to both vibratory motion of flexible modes and rigid-body motion. Accordingly, the total generalised force vector is expressed as:

$$f(t)=\mathbf{f}_{\mathbf{flex}}(t)+\mathbf{f}_{\mathbf{rigid}}(t) \qquad \ldots(2)$$

where $\mathbf{f}_{\mathbf{flex}}$ is the generalised aerodynamic force vector acting on the flexible modes and $\mathbf{f}_{\mathbf{rigid}}$ is the generalised force vector due to rigid-body motion.

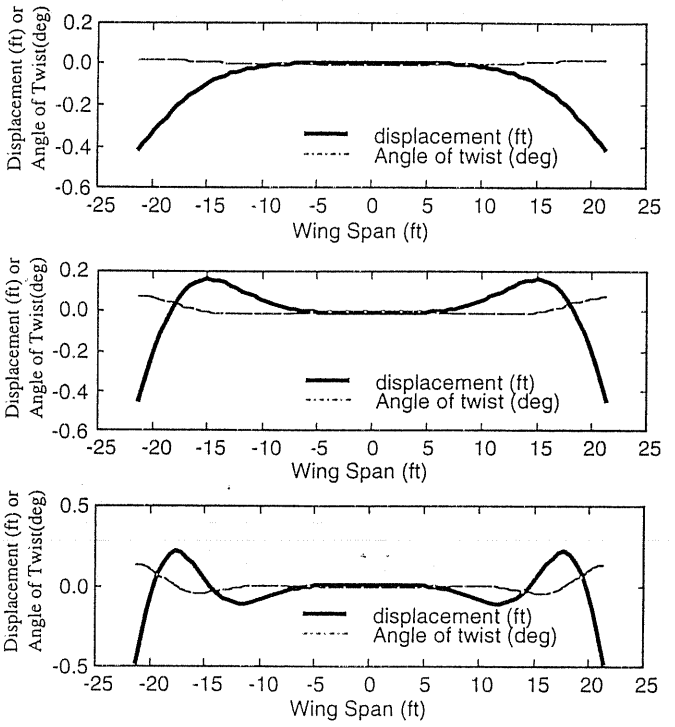

Figure 2. First three symmetric mode shapes.

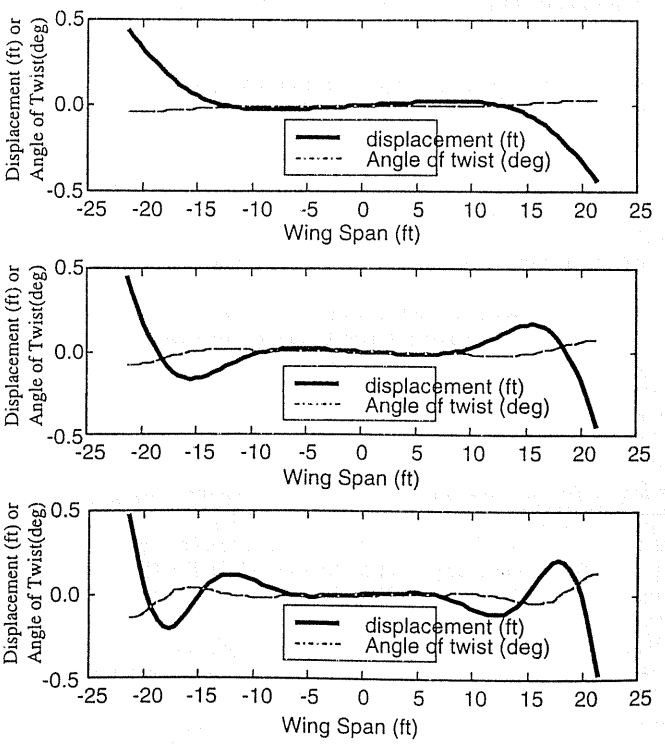

Figure 3. First three antisymmetric mode shapes.

For the specific wing structure considered in this paper, we have used the six lowest modes, of which three are symmetric and three are antisymmetric with respect to the aircraft body-fixed x-axis. Figures 2 and 3 show the symmetric mode shapes and the antisymmetric mode shapes for both linear displacement and angular twist. It is necessary to make the distinction between symmetric and antisymmetric modes because the dynamics of the two sets of modes are decoupled from each other. Within each set of symmetric and antisymmetric modes, however, the dynamics are coupled due to the aerodynamic forces generated by wing deformation.

2.5 Integrated model of unsteady aerodynamics and structural dynamics

Although the current state-of-the-art in computational fluid dynamics (CFD) allows time-domain solutions to the Euler equations (for inviscid compressible flow) or the Navier-Stokes equations (for viscous compressible flow) for many flows of practical interest, the use of these techniques is still rather limited due to high computational cost. Within the aerospace industry, a vast majority of unsteady flow applications, such as flutter analysis, rely on computational techniques that have been developed for the restricted case of thin wings undergoing simple harmonic motion for unsteady subsonic potential flow[23]. The doublet-lattice method[24] has been adopted in this paper for aerodynamic analysis. In this method, the wing model is divided into a finite number of trapezoidal segments. The lifting force acting on each segment is assumed to be concentrated along the one-quarter chord line of the segment, where a line of acceleration potential doublets is placed. The strength of the doublets is assumed to be uniform within each panel segment and is allowed to vary from one segment to the next. A control point is placed at the three-quarter-chord point of the mid-span of each segment. Details are reported by Caplin[22].

The transfer matrix from the generalised displacement vector to the flexible part of the total generalised force vector is approximated as a function of the dimensionless Laplace transform variable s and dynamic pressure q[25]:

$$Q(s) \approx \left(\mathbf{A}_0 + \bar{s}\mathbf{A}_1 + \bar{s}^2\mathbf{A}_2 + \bar{s}\mathbf{D}(\bar{s}I - \mathbf{R})^{-1}\mathbf{E}\right)\bar{q};$$
$$\bar{s} \equiv \frac{sb}{U_\infty}; \bar{q} \equiv \frac{1}{2}\rho_\infty (U_\infty)^2 \quad \ldots (3)$$

where U_∞ and ρ_∞ are the undisturbed free-stream air flow speed and density, respectively; b is the wing semi-span; the matrix $\mathbf{A}_0$ is obtained from the steady-sate response of experimental or CFD simulation data; other matrices $\mathbf{A}_1$, $\mathbf{A}_2$, $\mathbf{D}$ and $\mathbf{E}$ are obtained by frequency-domain system identification based on experimental or CFD simulation data; and is a diagonal matrix whose elements are chosen to be the poles of additional aerodynamic states within the frequency range of interest.

Remark: The terms involving the matrices A_0, A_1 and A_2 in Equation (3) capture the dependence of the aerodynamic forces on the displacement, velocity, and acceleration, respectively, of the wing mode shapes. The remaining term, involving the matrices **D**, **R** and **E** on the right hand side of Equation (3), account for the lag in aerodynamic forces.

Transforming Equation (3) into the time domain and substituting the resulting expression into Equations (1) and (2) yield the following set of ordinary differential equations:
where $\mathbf{x}_a$ is the vector of selected states to represent the aerodynamic lag;

$$M\ddot{\xi}(t) + C\dot{\xi}(t) + K\xi(t) =$$
$$\left(\mathbf{A}_0\xi(t) + \frac{b}{U_\infty}\mathbf{A}_1\dot{\xi}(t) + \left(\frac{b}{U_\infty}\right)^2\mathbf{A}_2\ddot{\xi}(t) + \mathbf{D}\mathbf{x}_a(t)\right)\bar{q} + \mathbf{f}_{rigid}(t) \quad \ldots (4)$$
$$\frac{\mathrm{d}}{\mathrm{d}t}(\dot{\mathbf{x}}_a(t)) = \mathbf{E}\dot{\xi}(t) + \frac{U_\infty}{b}\mathbf{R}\mathbf{x}_a(t)$$

and $\mathbf{f}_{rigid}$ is the part of the total generalised force vector contributed by the rigid-body motion as defined in Equation (2). The aeroelastic model in Equation (4) is rewritten in the state space setting for synthesis of life-extending controllers as:
by introducing the following definitions:

$$\frac{\mathrm{d}}{\mathrm{d}t}(\xi(t)) = \dot{\xi}(t)$$
$$\frac{\mathrm{d}}{\mathrm{d}t}(\dot{\xi}(t)) = \bar{M}^{-1}\left(-\bar{K}\xi(t) - \bar{C}\dot{\xi}(t) + \bar{q}\mathbf{D}\mathbf{x}_a(t) + \mathbf{f}_{rigid}(t)\right) \quad \ldots (5)$$
$$\frac{\mathrm{d}}{\mathrm{d}t}(x_a(t)) = E\dot{\xi}(t) + \frac{U_\infty}{b}R\mathbf{x}_a(t)\xi$$

The aeroelastic model in Equation (5) forms two uncoupled sets of

$$\bar{M} \equiv M - \left(\frac{b}{U_\infty}\right)^2\bar{q}\mathbf{A}_2; \bar{C} \equiv C - \frac{b}{U_\infty}\bar{q}\mathbf{A}_1; K \equiv \bar{K} - \bar{q}\mathbf{A}_0 \quad \ldots (6)$$

equations, one for the symmetric modes and the other for the antisymmetric modes. Additional aerodynamic terms representing $\mathbf{f}_{rigid}$ in Equation (5) must be added to each model to account for the relevant rigid-body motions. Furthermore, the perturbations in the rigid-body aerodynamic coefficients are different for each model. These considerations are addressed in the next two sections.

2.6 Symmetric Aeroelastic Model

In general, the largest contribution to the aerodynamic loads acting on the wing is due to the rigid-body angle-of-attack. Strictly speaking, this requires addition of three terms to Equation (5); one for the angle-of-attack, and one each for its first two derivatives. However, it is generally recognised that terms involving the second derivative of the rigid body motion may be neglected for characteristic frequencies below 2Hz. Since angle-of-attack α does not have any significant frequency content above 2Hz, the term involving the acceleration has not been included in the complete aeroelastic model.

Two inertial terms, $Q_{a_z}a_z(t)$ and $Q_{\dot{q}}\dot{q}(t)$, which are proportional to normal acceleration and pitch acceleration of the aircraft, respectively, are added to the model when longitudinal rigid-body motion is considered. Substituting these inertial terms along with additional aerodynamic terms into Equation (5) yields the following set of equations for the symmetric aeroelastic model:
The main effect of symmetric deformation of the wing on the overall

$$\frac{\mathrm{d}}{\mathrm{d}t}(\xi(t)) = \dot{\xi}(t)$$
$$\frac{\mathrm{d}}{\mathrm{d}t}(\dot{\xi}(t)) = \bar{M}^{-1}\left(\begin{array}{l} -\bar{K}\xi(t) - \bar{C}\dot{\xi}(t) + \\ \left(\mathbf{A}_\alpha\alpha(t) + \frac{b}{U_\infty}\mathbf{A}_{\dot{\alpha}}\dot{\alpha}(t) + \mathbf{D}\mathbf{x}_a(t)\right)\bar{q} + \\ Q_{az}a_z(t) + Q_{\dot{q}}\dot{q}(t) \end{array}\right) \quad \ldots (7)$$
$$\frac{\mathrm{d}}{\mathrm{d}t}(x_a) = \mathbf{E}\dot{\xi}(t) + \frac{U_\infty}{b}\mathbf{R}x_a(t) + \mathbf{E}_{\dot{\alpha}}\dot{\alpha}(t)$$

dynamics of the aircraft is assumed to be due to the change in lift coefficient. The transfer function from generalised displacement to change in lift coefficient is obtained in the same manner as the transfer function from generalised displacement to generalised force. Thus the unsteady perturbation in lift coefficient is obtained in the time-domain as:

$$\Delta C_L(t) = \mathbf{A}_{0C_L}\xi(t) + \frac{b}{U_\infty}\mathbf{A}_{1C_L}\dot{\xi}(t)$$
$$+\left(\frac{b}{U_\infty}\right)^2\mathbf{A}_{2C_L}\ddot{\xi}(t) + \mathbf{D}_{C_L}\mathbf{x}_a(t) \quad \ldots (8)$$

2.7 Antisymmetric aeroelastic model

Two additional sets of aerodynamic terms are added to the antisymmetric model. First, deflection $\delta_A(t)$ of the ailerons is viewed as an additional deformation mode of the wing, and thus additional aerodynamic terms involving aileron position, rate, and acceleration must be included. Second, terms involving the rigid-body roll rate and roll acceleration are required although roll angle has no effects. Only one inertial term, $Q_{\dot{p}}\,\dot{p}\,(t)$, which is proportional to roll acceleration of the aircraft, is added to the model when lateral rigid-body motion is considered. The antisymmetric aeroelastic model thus takes the following form:

$$\frac{\mathrm{d}}{\mathrm{d}t}(\eta(t)) = \dot{\eta}(t)$$

$$\frac{\mathrm{d}}{\mathrm{d}t}(\dot{\eta}(t)) = \overline{M}^{-1}\left(-\overline{K}\eta(t) - \overline{C}\dot{\eta}(t) + \bar{q}\mathbf{D}y_a(t) + Q_{\dot{p}}\dot{p}(t)\right)$$

$$+\overline{\overline{M}}^{-1}\left[\begin{array}{l}\mathbf{A}_{\delta_A}\delta_A(t) + \dfrac{b}{U_\infty}\mathbf{A}_{\dot{\delta}_A}\dot{\delta}_A(t) + \\ \left(\dfrac{b}{U_\infty}\right)^2\mathbf{A}_{\ddot{\delta}}\ddot{\delta}_A(t) + \dfrac{b}{U_\infty}\mathbf{A}_p p(t) + \left(\dfrac{b}{U_\infty}\right)^2\mathbf{A}_{\dot{p}}\dot{p}(t)\end{array}\right]\bar{q} \qquad \ldots (9)$$

$$\frac{\mathrm{d}}{\mathrm{d}t}(y_a) = \mathbf{E}\dot{\eta}(t) + \frac{U_\infty}{b}\mathbf{R}y_a(t) + \mathbf{E}_{\dot{\delta}_A}\dot{\delta}_A(t) + \mathbf{E}_p p(t)$$

where the symbols η and γ have been used for the generalised displacement vector and the aerodynamic state, respectively, in order to distinguish the antisymmetric states from the symmetric states ξ and $\mathbf{x}_a$. The main effect of antisymmetric deformation of the wing on the overall dynamics of the aircraft is due to the change in roll moment coefficient. Its transfer function with respect to generalised displacement is obtained similar to Equation (8). Thus the unsteady perturbation in the roll moment coefficient is obtained in the time-domain as:

$$\Delta C_l(t) = \mathbf{A}_{0_{Cl}}\eta(t) + \frac{b}{U_\infty}\mathbf{A}_{1_{Cl}}\dot{\eta}(t) + \left(\frac{b}{U_\infty}\right)^2\mathbf{A}_{2_{Cl}}\ddot{\eta}(t) + \mathbf{D}_{Cl}y_a(t) \qquad \ldots (10)$$

Remark: The major effect of antisymmetric deformation of the wing on the overall dynamics of the aircraft is due to the change in roll moment coefficient.

2.8 Propulsion system model

The propulsion system model is based on the data for an F100 turbofan engine installed in the F-15 aircraft. The steady-state values for idle, military, and maximum afterburner thrust are tabulated as functions of Mach number, altitude, and power lever angle (PLA). The model includes first-order core dynamics, with a time constant computed via linear interpolation as a function of percent military thrust, Mach number, and altitude. The afterburner model includes sequencing logic to handle the transitions between the afterburner stages.

2.9 The state-space model of fatigue crack damage

In general, airframe structures are made of aluminum alloys that are always subjected to very small cracks in addition to material impurities such as voids and inclusions. As such the crack growth phenomena in the critical structures such as the wing root is sensitive to stress overload in the following sense. While large cyclic loads of constant-amplitude are detrimental to structural durability, researchers[26] in the field of fracture mechanics discovered that short-duration overloads on small or medium cyclic loads of constant-amplitude could, in fact, extend the fatigue life. This claim has been experimentally validated on fatigue testing machines[27,28]. The rationale for this physical phenomenon is that an overload enlarges the plastic zone at the crack tip, which, in turn, causes compressive forces to act on the plastic zone around the crack tip region. Thus, crack growth is retarded due to an increase in the crack opening stress. Along this line, Patankar and Ray[6] have formulated a state-space model of fatigue crack growth for life-extending controller analysis and synthesis that accounts for the impact of variable-amplitude loading on crack growth rate (e.g. crack retardation and sequence effects). Patankar and Ray[6] have also shown that the predicted structural durability (and hence the controller design) could be grossly inaccurate if the fatigue crack damage model does not capture the effects of variable-amplitude cyclic stress.

Different aspects of fatigue crack damage have been reported by many investigators as cited in research monographs[29][5]) on fracture mechanics. In the present paper, we have used the fatigue crack growth model of Patankar and Ray[6] in the state-space setting to allow its incorporation in the aircraft control system model. The state-space model of fatigue crack damage has been validated with the test data of McMillan and Pelloux[27] and Porter[28] along with explanations of the underlying physical phenomena. The model is an extension of the Fastran model[30,31] which is based on the concept of small cracks in homogeneous materials. The Fastran model is represented by a nonlinear difference equation in which the crack increment during the k^{th} cycle is obtained as a function of the maximum applied (far-field) stress $s_k^{\max}$ and the crack opening stress s_k^0 as:

$$\left.\begin{array}{l}\Delta a_k \equiv a_k - a_{k-1} = h\left(K_k^{eff}\right) \quad \text{with } h(0) = 0 \\ \Delta K_k^{eff} \equiv \sqrt{a_{k-1}}\,F\left(a_{k-1}, \tilde{w}\right) \\ \left(S_k^{\max} - S_{k-1}^{\max}\right)U\left(S_k^{\max} - S_{k-1}^0\right)\end{array}\right\} \begin{array}{l}for\ k \geq 1 \\ and\ a_0 > 0\end{array} \qquad \ldots (11)$$

where x_{k-1} and s_{k-1}^0 are the crack-length and the crack-opening stress, respectively, during the k^{th} cycle and change to a_k and s_k^0 at the expiry of the k^{th} cycle; $F(\bullet,\bullet)$ is a crack-length-dependent correction factor compensating for finite geometry of the specimen with the width parameter $\tilde{w}$; the non-negative monotonically increasing function $h(\bullet)$ can be represented either by a closed form algebraic equation:

$$h\left(\Delta K_k^{eff}\right) = \mathrm{C_1}\left(\Delta K_k^{eff}\right)^{\mathrm{m}} \text{ with material constants } \mathrm{C_1} \text{ and m,} \qquad \ldots (12)$$

or by table lookup[31]; and $U(x) = \begin{cases} 0 \ if\ x < 0 \\ 1 \ if\ x \geq 0 \end{cases}$ is the Heaviside function.

We now present the structure of the difference equation that is excited by the cyclic stress input to generate the crack opening stress. To this end, we first consider the steady-state solution of the difference equation under constant amplitude load. This issue has been addressed by several investigators including Newman[32] and Ibrahim et al[33]. The steady-state crack-opening S^{oss} stress under a constant amplitude cyclic load is a function of the minimum stress $S^{\min}$, the maximum stress $S^{\max}$, the constraint factor α (which is 1 for plane stress and 3 for plane strain), the specimen geometry, and the flow stress S^{flow} (which is the average of the yield strength S^y and the ultimate strength S^{ult}). These relationships are shown to be good for most ductile alloys by Newman[32].

The objective is to construct the difference equation for (non-negative cycle-dependent) crack opening stress s_k^o such that, under different levels of constant-amplitude load, the forcing function s_k^{oss} at the k^{th} cycle matches the crack-opening stress derived from the following empirical relation[31] that is valid for non-zero peak stress (i.e. $S^{\max} \neq 0$):

$$S_k^{oss} = S^{oss}\left(S_k^{\max}, S_k^{\min}, \alpha, F\right) = \left(\tilde{\mathbf{A}}_k^0 + \tilde{\mathbf{A}}_k^1\mathbf{R}_k + \tilde{\mathbf{A}}_k^2(\mathbf{R}_k)^2 + \tilde{\mathbf{A}}_k^3(\mathbf{R}_k)^3\right)S_k^{\max} \qquad \ldots (13)$$

where $\mathbf{R}_k = \dfrac{S_k^{\min}}{S_k^{\max}}U\left(S_k^{\max}\right)$ for all $k \geq 0$;

$$\tilde{A}_k^0 = \left(0\cdot825 - 0\cdot34\alpha_k + 0\cdot05(\alpha_k)^2\right)\left[\mathrm{Cos}\left(\frac{\pi}{2}\frac{S_k^{max}}{S^{flow}}F(a_{k-1},\tilde{w})\right)\right]^{1/\alpha_k} \quad \ldots(15)$$

$$\tilde{A}_k^1 = 0\cdot415 - 0\cdot071\alpha_k\left(\frac{S_k^{max}}{S^{flow}}F(a_{k-1},\tilde{w})\right) \quad \ldots(16)$$

$$\tilde{A}_k^2 = \left(1 - \tilde{A}_k^0 - \tilde{A}_k^1 - \tilde{A}_k^3\right)U(R_k) \quad \ldots(17)$$

$$\tilde{A}_k^3 = \left(2\tilde{A}_k^0 + \tilde{A}_k^1 - 1\right)U(R_k) \quad \ldots(18)$$

The constraint factor α_k used in Equations (15) and (16) is obtained as a function of the crack length increment Δa_k in Equation (11). A procedure for evaluation of α_k is presented in the Fastran manual[31]. Since α_k does not significantly change over cycles, it can be approximated as piecewise constant for limited ranges of crack length.

The following constitutive relation, in the form of a nonlinear first order difference equation, recursively calculates the crack-opening stress S_k^o upon completion of the k^{th} cycle[6]:

$$S_k^0 = \left(\frac{1}{1+\eta}\right)S_{k-1}^0 + \left(\frac{1}{1+\eta}\right)\left(S_k^{oss}\right) + \left(\frac{1}{1+\eta}\right)\left(S_k^{oss} - S_{k-1}^{oss}\right)U\left(S_k^{oss} - S_{k-1}^{oss}\right) + \left(\frac{1}{1+\eta}\right)\left[S_k^{oss} - S_k^{oss\_old}\right]U\left(S_{k-1}^{min} - S_k^{min}\right)\left[1 - U\left(S_k^{oss} - S_{k-1}^{oss}\right)\right] \quad \ldots(19)$$

$$\eta = \frac{tS^y}{2\tilde{w}E} \quad \ldots(20)$$

where the forcing function S_k^{oss} in Equation (19) is calculated from Equation (13) as if a constant amplitude stress cycle (S_k^{max}, S_k^{max}) is applied; similarly, $S_k^{oss\_old}$ is given by Equation (13) as if a constant amplitude stress cycle $(S_k^{max}, S_{k-1}^{min})$ is applied. For constant-amplitude loading, is the steady-state solution of S_k^o. In general, the inputs S_k^{oss} and $S_k^{oss\_old}$ to Equation (19) are different from the instantaneous crack-opening stress S_k^o under variable-amplitude loading. The Heaviside function $U(S_k^{oss} - S_{k-1}^o)$ in the third term on the right hand side of Equation (19) allows fast rise and slow decay of S_k^o. The last term on the right hand side of Equation (19) accounts for the effects of reverse plastic flow. Depletion of the normal plastic zone occurs when the minimum stress S_k^{min} decreases below its value S_{k-1}^{min} in the previous cycle, which is incorporated via the Heaviside function $U(S_{k-1}^{min} - S_k^{min})$. Note that the overload excitation and reverse plastic flow are mutually exclusive.

The dimensionless parameter η in Equation (20) depends on the component thickness t, half-width w, yield strength S^y, and Young's modulus E. Alternatively, Equation (10) could be used to generate an estimate of η can be fine-tuned by parameter identification using available test data. Following an overload cycle, the duration of crack retardation is controlled by the transients of S_k^o in the state-space model, and hence determined by the stress-independent parameter η in Equations (19) and (20). Physically, this duration depends on the ductility of the material that is dependent on many factors including the heat treatment of specimens[26]. Smaller yield strength produces a smaller value of η, resulting in longer duration of the overload effect. Smaller specimen thickness has a similar effect[26]. Equations (11) to (20) describe the state-space model where the crack length a_k and crack opening stress S_k^o are the state variables.

Remark: The net effect of a single-cycle overload (i.e. increased S_k^{max}) is a jump in the effective stress range $\Delta S_k \equiv S_k^{max} - S_k^o$ resulting in an increase in the crack growth increment in the present cycle. Shortly after the expiration of the overload (i.e., S_k^{max} returning to the original lower value), S_k^o starts decreasing slowly from its increased value. The result is a decrease in ΔS_k, which causes the crack growth rate to diminish. Subsequently, after returning to the original constant-amplitude stress, as S_k^o slowly relaxes back to its original state, the crack growth rate resumes the original value. A single overload initially increases crack growth rate for a few cycles and then gradually decreases over a much higher number of cycles until it reaches the original value. The crack growth is therefore retarded due to the fast rise and slow decay of S_k^o.

For any manoeuvre involving lateral motion of the aircraft, the stress profiles from the left and right wings are different. It is assumed that, on the average, a pilot would fly equal numbers of left turns and right turns, and similarly would not favour any particular direction for other manoeuvres. For this reason, when evaluating crack growth, the stress profiles from the left and right wings were strung together to form one block of cyclic stress profile and are referred to as a single manoeuvre in Section 4.2. Thus, crack growth results apply equally to both wings.

2.10 Life extending control system

The objective of life extending control (LEC) is to inhibit or reduce fatigue crack growth in the wing structure. Figure 4 shows a schematic representation of the LEC system in which the controller acts upon the subsystem models, described above, with the exception of the fatigue crack growth model that is placed outside the feedback control loop solely for the purpose of on-line damage monitoring.

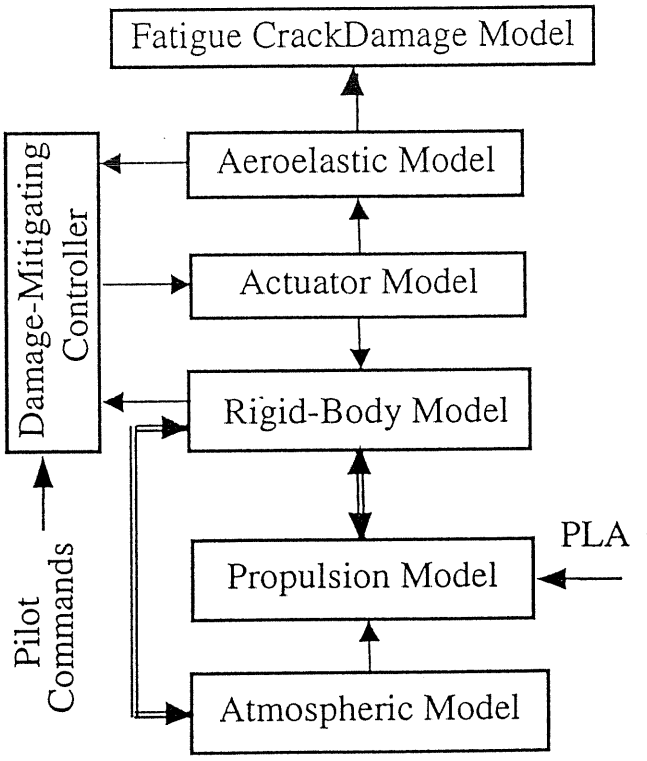

Figure 4. Damage mitigating control system schematic.

Although the state-space structure of the fatigue crack growth model allows its incorporation within the control system and fatigue crack damage is a combined effect of both lateral and longitudinal motions, we have separately designed robust linear controllers for these motions. The rationale for this approach is that the damage rate bears a strong nonlinear relationship with strain in the airframe structures and hence cannot be handled by linear techniques. Holmes and Ray[9] and Lorenzo *et al*[34] have addressed this issue in a two-tier architecture for damage-mitigating control of rocket engines in which the damage information is utilised for the outer loop and the linear controller in inner loop guarantees robust stability. The nonlinear relationship between strain and fatigue crack growth rate is not directly handled by the controller synthesis procedure presented in this paper.

3.0 ROBUST LIFE EXTENDING CONTROL SYNTHESIS

The H_∞–based structured singular value (μ) synthesis technique[35] has been chosen as the robust controller design method in this paper. Since aircraft controllers are increasingly being implemented on digital computers, sampled-data control systems have been designed using the function *sdhfsyn* in the MATLAB mutools toolbox[36] that is based on the methods of Bamieh and Pearson[37] and Shivashanker and Khargonekar[38]. As mentioned earlier, separate robust controllers are designed for the lateral and longitudinal motion of the aircraft.

Next we describe the generalised plant models (i.e. the augmented system of the aircraft dynamics, actuator dynamics, plant modelling uncertainties, and performance weighting functions) used for synthesis of the longitudinal and lateral controllers, respectively. Note that the output of the crack-growth model is not used for feedback into the controller in either case. This paper focuses on robust control of flight dynamics in which the damage model is used only for analysis of the controller as well as for understanding the physical relationship between flight dynamics and fatigue crack growth. Nevertheless, the proposed control system has the flexibility of incorporating the output of the damage model as a feedback signal in an outer control loop following the architecture of Holmes and Ray[9] and Lorenzo *et al*[34].

3.1 Lateral motion controller synthesis

The state vector used for synthesis of the lateral controller includes both the lateral rigid-body states and the states of the antisymmetric aeroelastic model. Since the spiral mode is not of interest during the controller synthesis phase, it is possible to neglect the role angle state without significantly altering the dynamics of the other modes. Thus, by considering the first three degrees of freedom for generalised displacements and n additional aerodynamic states of the antisymmetric aeroelastic model in Equation (8), the plant state vector of lateral motion becomes:

$$\mathbf{x}_{lat} = [p \;\; r \;\; \beta \;\; \eta_1 \;\; \eta_2 \;\; \eta_3 \;\; \dot{\eta}_1 \;\; \dot{\eta}_2 \;\; \dot{\eta}_3 \;\; y_1^a \;\; \ldots \;\; y_n^a]^T \quad \ldots (21)$$

where

p is the roll rate;
r is the yaw rate;
β is the sideslip angle;
η_k, k = 1,2,3 are the coefficients of the first three antisymmetric modes of structural deformation;
$\dot{\eta}_k$, k = 1,2,3 are the time derivatives of η_k, k= 1,2,3, respectively;
η_{ak}, k = 1,2,3(we have chosen n = 8 in this paper) are aerodynamic states chosen for the antisymmetric aeroelastic model.

The generalised plant used for synthesis of the lateral controller is shown in Fig. 5. The ideal model contains two blocks; one is a unity-gain first order system representing the desired roll mode time constant 0·33 sec, and the other block is a second order linear time-invariant system with the desired natural frequency 3 rad/sec and damping ratio 0·707, of the Dutch roll mode. The performance weighting function $W_p(s)$ contains three blocks.

The first two blocs, $\dfrac{0{\cdot}005(s+500)}{(s+0{\cdot}1)}$ and $\dfrac{0{\cdot}002(s+5000)}{(s+10)}$, penalise the differences in roll rate and sideslip responses of the aircraft model and the ideal model. The third block penalises the difference in bending strain between the left and right wings. Although the wings are subjected to both bending and torsional displacements, the magnitude of the torsional strain is about two orders of magnitude lower than the

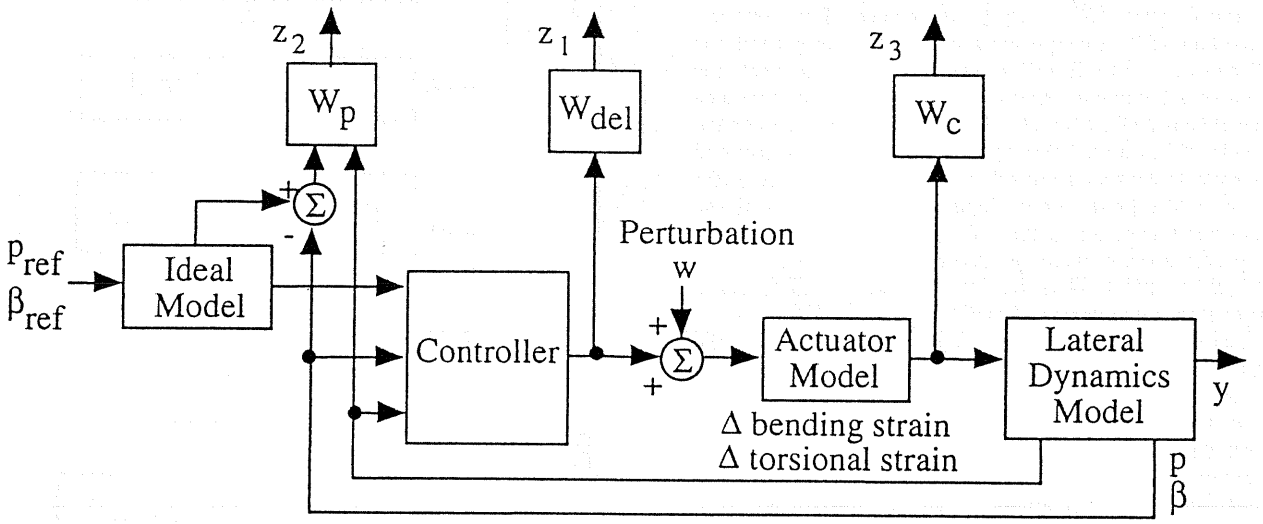

Figure 5. Generalised plant model for lateral controller design.

Controller	Strain weighting function	Weighting function type
LEC1	10	All-pass
LEC2	$\frac{10^7(s+10)}{s^2+10^4 s+10^7}$	Band-pass

Table 2
Strain weighting functions used in lateral controller synthesis

bending strain. Thus, the principal strain is essentially equal to the bending strain, and only the bending strain is penalised during controller synthesis. However, both values are used as feedback signals for control purposes. The strain weighting functions are selected for the life-extending controller design based on the information generated from extensive simulation runs. Two different choices of the strain weighting function are given in Table 2. The transfer function $W_c(s)$ represents the frequency-dependent weights placed on the antisymmetric stabilator deflection and its rate. These weights are constant over the frequency range of interest, and are chosen to be the inverses of the maximum position and rate. The low-pass filter on the reference signal is included to make the D-matrix of the generalised plant zero, which is a requirement of the MATLAB function *sdhfsyn* for sampled data controller design. The transfer function $W_{del}(s)$ is the uncertainty weight. In an actual design case, it would be desirable to characterise the uncertainty in the plant model based on the known dynamic behaviour of the aircraft, preferably from experimental data. In this case, since the model[17] does not represent any specific aircraft, no such data was available. Therefore,

we have chosen an uncertainty weight of $\frac{20000(s+100)}{(s+2000)(s+10000)}$,

which represents ~10% uncertainty at low frequencies increasing to ~200% uncertainty at high frequencies. For the lateral model it is found that good results can be obtained when the ideal models are also used as the low-pass filters on the reference signals. This choice slightly reduces the order of the generalised plant.

3.2 Longitudinal controller synthesis

The state vector used for synthesis of the longitudinal controller includes both the longitudinal rigid-body states and the states of the symmetric aeroelastic model. However, since the phugoid mode is not of interest, it is possible to ignore the velocity, altitude, and pitch angle states without significantly altering the short period response of the aircraft. Thus, by considering the first three degrees of freedom for generalised displacements and ℓ additional aerodynamic states of the symmetric aeroelastic model in Equation (6), the plant state vector of longitudinal motion becomes:

$$\mathbf{x_{long}} = [q \;\; \alpha \;\; \xi_1 \;\; \xi_2 \;\; \xi_3 \;\; \dot{\xi}_1 \;\; \dot{\xi}_2 \;\; \dot{\xi}_3 \;\; x_{a1} \;\; \cdots \;\; x_{a_\ell}]^T \quad \ldots (22)$$

where

q is the pitch rate;
α is the angle-of-attack;
ξ, k = 1,2,3 are the coefficients of the first three symmetric modes of structural deformation;
$\dot{\xi}_k$, k are the time derivatives of ξ_k, k = 1,2,3 respectively;
x_{a_k}, k = 1,2,···, ℓ (we have chosen ℓ =8 in this paper) are the aerodynamic states chosen for the symmetric aeroelastic model.

The generalised plant used for synthesis of the longitudinal controller is shown in Fig. 6. The ideal model is selected to be a 5 rad/sec and damping ratio 0·8 to match the desired short period response of the aircraft. The performance weighting function $W_p(s)$ contains two blocks.

The first block $\frac{0.25(s+200)}{(s+5)}$ penalises the difference in pitch rate response between the outputs of the aircraft model and the ideal model. The second block penalises the average bending strain of the left and right wings. Two different choices of the strain weighting function are given in Table 2. The frequency-dependent weight $W_c(s)$ penalises the actuator positions and rates of the symmetric stabilator deflection and its rate. Similar to the lateral controller, these weights are constant over the frequency range of interest, and are chosen to be the inverses of the maximum position and rate. The transfer function $W_{del}(s)$ is the uncertainty weight, which is the same as that used for the lateral controller design.

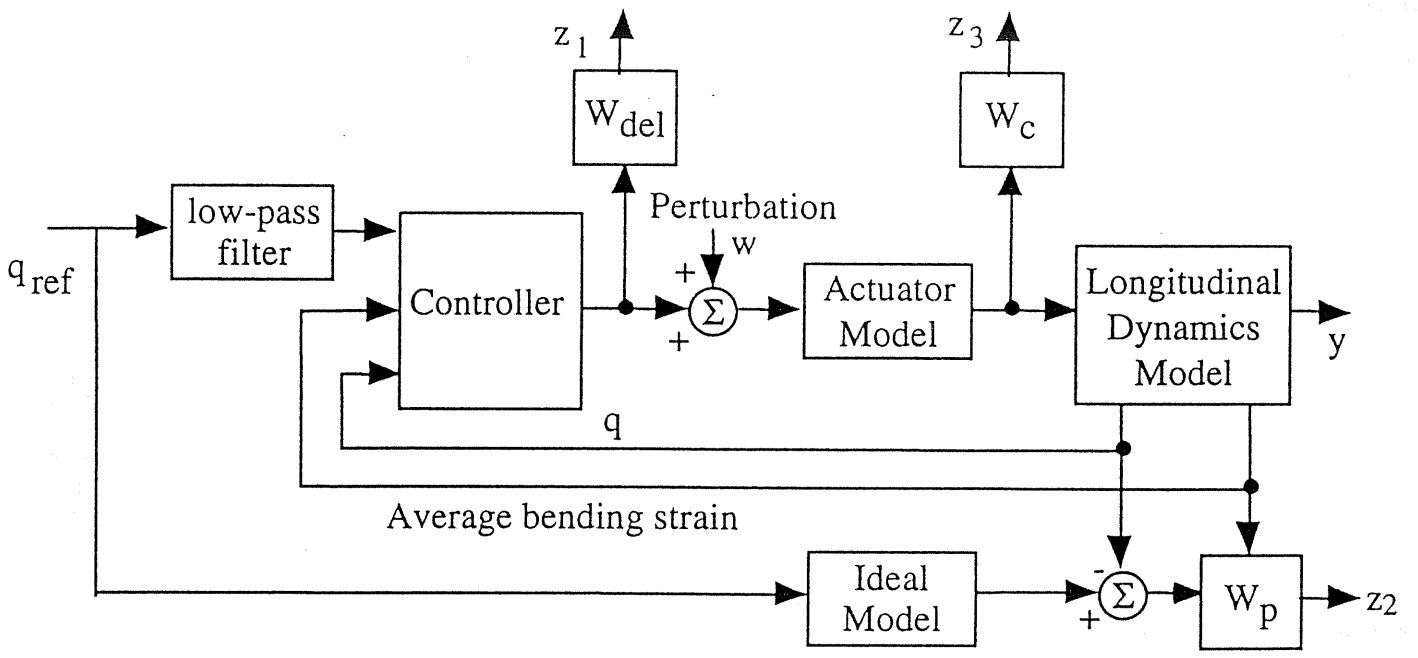

Figure 6. Generalised plant model for longitudinal controller design.

Remark: For synthesis of linear control laws, the performance optimisation must be carried out in terms of measurable quantities whose behaviour can be captured by a linear model. The far-field strains near the critical point of each wing have been chosen for this purpose.

Remark: Frequency-dependent weighting functions are chosen for penalising the average strain and the difference in strain at the critical points of the left and right wings. Due to the nonlinear relationship between strain and fatigue crack growth rate, the desired forms of the weighting functions are not known a priori. The existing literature does not address this issue of strain weighting with the exception of Holmes and Ray[9] who have not adequately included the effects of variable amplitude loading in the fatigue crack growth model.

4.0 EVALUATION OF THE LIFE EXTENDING CONTROL SYSTEM

There are a few issues that need to be addressed for evaluation of life extending (i.e., damage mitigating) capabilities of an aircraft controller. First, it is necessary to ensure that comparable rigid-body motions are executed with each simulation run. For example, it would not be meaningful to compare crack growth for one manoeuvre having a peak load factor of 8g with that from an almost similar manoeuvre in which the peak load factor is, say, 7g. The second issue is how to compare the results of crack growth from different simulation runs with due consideration to the effects of variable-amplitude cyclic stresses. The third issue is evaluation of crack growth due to multi-axial stresses resulting from combined actions of the lateral and longitudinal controllers. Although the lateral and longitudinal dynamics of the aircraft are very weakly coupled and the respective controllers are designed separately, the fatigue crack damage depends on the total stress at the crack tip, to which both the symmetric and antisymmetric aeroelastic models make contributions. The controller design procedure should be a three-step process from these perspectives:

Step#1: Evaluate all longitudinal life extending controllers while the aircraft simulation model is executed for purely longitudinal manoeuvres. Alternatively, one could lift the restriction on pure longitudinal motion as long as the same lateral controller is used in all cases.

Step#2: Evaluate all lateral life extending controllers while the aircraft simulation model is executed for combined lateral-longitudinal manoeuvres using the same longitudinal controller. Limiting the manoeuvres to pure lateral motion would also be an option for aircraft that are not designed for aggressive manoeuvres. For fighter aircraft, however, the average stresses experienced under pure lateral motion would most likely be too far below the maximum allowable stresses for any significant fatigue crack growth to be observed.

Step#3: After selecting one or more potential candidates from each of the previous two steps, the candidate lateral and longitudinal Life Extending Controllers must be evaluated in pairs under combined lateral and longitudinal manoeuvreing.

In this paper, however, no significant damage-mitigation is achieved with the longitudinal controller. Therefore, Step#3 is deemed unnecessary for this aircraft. Furthermore, since the bending stresses dominate the torsional stresses, fatigue damage is calculated based on the assumption of uniaxial (bending) stresses.

4.1 Evaluation of fatigue crack damage

The fatigue life of a structure depends not only on the applied load profile but also on the initial condition of the crack damage in the structure. Starting with the same initial crack length, differences in crack growth profiles from different simulation runs can therefore be attributed solely to the actions of different controllers. Comparisons could then be made between the different controllers based on the number of manoeuvres required for the crack length to reach a specified final crack length. For any manoeuvre involving lateral motion of the aircraft, although the stress profiles from the left and right wings are different, crack growth results apply to both wings. Over a flight mission, the numbers of left turns and right turns are expected to be similar with no particular emphasis on the direction of manoeuvres. Therefore, for evaluation of crack damage, the stress profiles from the left and right wings are strung together to form a single block of (variable-amplitude) cyclic load corresponding to one average manoeuvre. The results are applicable to either wing — left or right.

4.2 Simulation results under life extending control

The longitudinal controller in the aircraft under consideration is provided with only one control input (i.e. symmetric stabilator deflection) for regulating both the rigid-body pitch rate and the average strain at the wing root. In addition, no direct control of the symmetric force distribution on the wing span is available as these forces can only be changed at the expense of the rigid-body motion that determines the aircraft performance. Since the requirements of handling qualities must be met at low frequencies (up to approximately 10 rad/sec), it would be unreasonable to influence the strain response within this frequency range. Thus, the only available choice for a strain weighting function is a band-pass filter. Several different filters were examined, however none seemed to have any significant effect on fatigue crack growth reduction without any significant loss of performance. The strain response was dominated by low frequencies, and the controller was unable to influence what little high-frequency content there was, due to the strict pitch rate response requirements. In the aircraft under consideration, the longitudinal controller is not very effective for damage mitigation. Therefore, we concentrate on the lateral controller in the sequel.

Since the aircraft under consideration is equipped with both ailerons and stabilators for roll control, the lateral controllers have the ability, within limits, to independently influence both the rigid-body roll rate and the stress transients in the wing. This allows examination of various types of strain weighting functions in the corresponding block of performance penalty transfer matrix **Wp(s)** in Fig. 5. In order to create a baseline case, one controller, denoted as the performance controller (PC) is synthesised without using any strain feedback or any penalty on the strain response. Additional strain weighting functions are provided for the lateral lateral-extending controllers (LECs). Two such LECs, called LEC1 and LEC2, are synthesised with different penalties on the strain response while the remaining weights are the same as those for the PC. Two basic types of strain weighting functions are investigated: an all-pass filter (constant weight), and a band-pass filter. Table 2 lists the strain weighting functions for LEC1 and LEC2. Both the PC and LECs are synthesised using a linearised model of the flexible aircraft in level, unaccelerated flight at an altitude of 5,000ft and a Mach number of 0·8. The results from a typical manoeuvre are presented below.

The turn reversal manoeuvre is selected for evaluating the damage-mitigating capabilities of the lateral controllers. Starting from level flight, the aircraft is rolled into a 7·5g turn to the right, then quickly reversed into an 8g turn to the left, and finally returned to straight and level flight The first three out of four plates in Fig. 7 show the roll rate, pitch rate, and sideslip angle transients, respectively, for the aircraft performing the turn reversal motion under the influence of each of three lateral controllers – PC, two — LECs (i.e. LEC1, and LEC2) along with the respective reference signals. The pitch rate of all three controllers is very close to the reference signal because this motion is largely governed by the longitudinal controller. The roll rate response of PC is practically identical to that of LEC1 and is slightly superior to that of LEC2. The sideslip response of PC is slightly superior to that of LEC1 while LEC2 shows larger deviations in the sideslip angle. The fourth plate in Fig. 7 compares the fatigue damage at the wing root under these three controllers. The fatigue damage in each case is computed by the state-space model based on the number of manoeuvres required for the crack length to reach 1mm starting from an initial value of 0·1mm. It

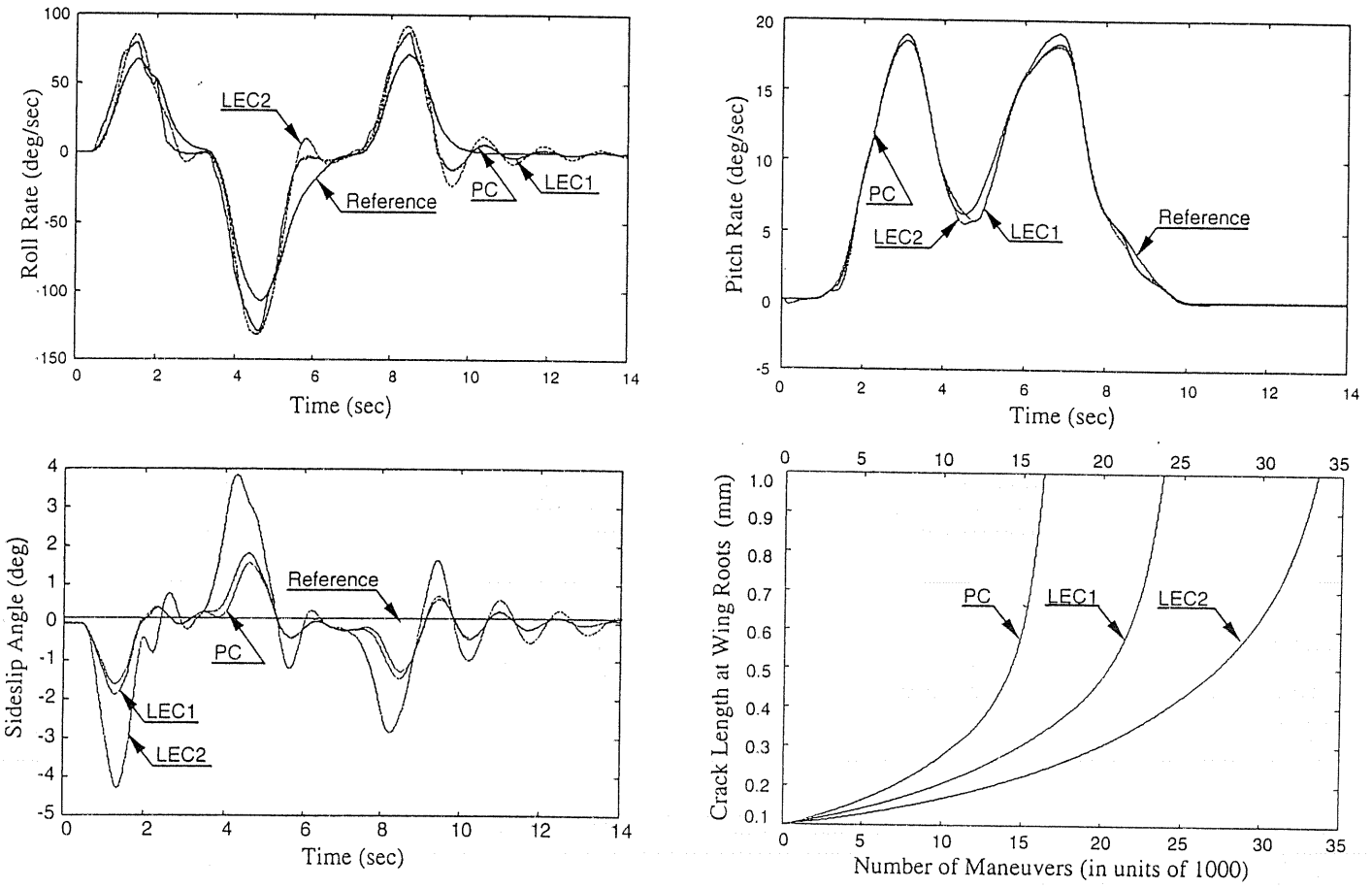

Figure 7. Aircraft performance and damage under turn reversal.

follows from Fig. 7 that LEC1 and LEC2 increase the fatigue life of wings by a factor of approximately ~140% and ~200%, respectively, over PC. Therefore, LEC1 yields ~40% saving in fatigue life with no apparent of loss of performance while LEC2 provides ~100% saving with noticeable increase in sideslip deviation.

5.0 SUMMARY AND CONCLUSIONS

This paper presents the synthesis of life-extending controllers (LECs) for high-performance tactical aircraft. Formulation of the control laws takes into consideration the impact of fatigue crack damage at critical points (e.g. wings) of aircraft structure, as well as the performance requirements. A flexible wing model is formulated using the finite element method, and the dominant mode shapes and natural frequencies are identified. The doublet-lattice method is employed to develop an unsteady flow model for computation of the time-dependent spatial aerodynamic loads acting on the wing due to rigid-body manoeuvres and structural deformation. The crack damage is calculated using a (nonlinear) state-space model of fatigue crack growth. These three models are subsequently incorporated into a pre-existing nonlinear rigid-body model of aircraft flight-dynamics. Robust life extending controllers are then designed using the H_∞–based structured singular value (μ) synthesis method based on a linearised model of the aircraft. In addition to penalising the error between the ideal performance and the actual performance of the aircraft, frequency-dependent weights are placed on the strain amplitude at the root of each wing. Using each controller in turn, the control system is put through an identical sequence of manoeuvres, and the resulting (varying amplitude cyclic) stress profiles are analysed using a fatigue crack growth model that incorporates the effects of stress overload. Comparisons are made to determine the impact of different weights on the resulting fatigue crack damage in the wings. The results of simulation experiments show that the LECs yield significant savings in fatigue life of the wing structure while retaining the dynamic performance of the aircraft. Specifically, the strain feedback is used for lateral motion control that manipulates the actuators (i.e. ailerons and stabilators) to simultaneously achieve high performance and damage mitigation.

Two important conclusions can be drawn from this research. The first is that life extending control of high-performance aircraft is achievable when redundant control surfaces are present. For the particular aircraft used in this paper, only the lateral controller was able to significantly influence fatigue crack damage in the wing due to its ability to allocate roll commands between the ailerons and the stabilators. Significant results could also be achieved with a longitudinal controller designed for an aircraft that has multiple control surfaces for longitudinal motion (such as canards, stabilators, leading-edge flaps, trailing-edge flaps, and thrust vectoring nozzles). Such a controller would be able to independently alter (within limits) the total lift and total pitching moment acting on the aircraft, and thus influence stresses in both the fuselage and the wings. The second and perhaps the more important conclusion is that LECs cannot be reliably synthesised when the analysis does not include adequate information on the dynamic behaviour of the crack-growth process[39]. Since, unlike aircraft engine components, airframe structures are always subjected to small cracks and material defects, stress overloads could be beneficial or harmful for airframe fatigue

life depending on their magnitude and frequency of occurrence as shown by experiments on a laboratory test apparatus[40]. This is contrary to the erroneous intuitive notion that reductions in peak stress will result in a reduction in damage. This is not necessarily true due to the effects of crack retardation.

Life extending control is capable of mitigating structural damage in aircraft structures with no significant loss of performance. The methodology can also be employed to the simultaneously design structural components and control systems for new aircraft, thus providing the structural engineers with more accurate information on the damage that critical components would experience in service. This information facilitates the design of less conservative structures, resulting in lighter-weight, higher-performance aircraft. The methodology can be extended to transport aircraft for both military and commercial applications.

The main application of this research is anticipated to be in the aircraft design phase, since this will allow the structural engineers and the control systems engineers to simultaneously converge to their individual goals of ensuring both performance and structural integrity of the aircraft. This approach will dramatically reduce the number of iterations required to arrive at a final design that can safely maximise the manoeuvreing capabilities of the aircraft.

REFERENCES

1. MATSUZAKI, Y., UEDA, T., MIYAZAWA, Y. and MATSUSHITA, H. Gust load alleviation of a transport-type wing: test and analysis, *J Airc*, 1989, **26**, (4), pp 322-327.
2. BALDELLI, D.H, OHTA, H. and NITTA, K. Gust load alleviation of an aeroelastic wing model, Transactions of the Japanese Society for Aeronautical and Space Sciences, 1993, **36**, (113), pp 125-142.
3. MCLEAN, D., *Automatic Flight Control Systems*, 1990, Prentice Hall International, London.
4. THORNTON, S.V. Reduction of structural loads using manoeuvre load control on the advanced fighter technology integration (AFTI)/F-111 mission adaptive wing, NASA TM-4526, 1993.
5. ANDERSON, T.L. *Fracture Mechanics, Fundamentals and Applications*, 1995, 2nd ed, CRC Press, Boca Raton.
6. PATANKAR, R. and RAY, A. State–space modelling of fatigue crack growth in ductile alloys, engineering fracture mechanics, 2000, **66**, pp 129-151.
7. RAY, A., WU, M-K., CARPINO, M. and LORENZO, C.F. Damage-mitigating control of mechanical systems: Parts I and II, *ASME J of Dynamic Systems, Measurement and Control*, 1994, **116**, (3), pp 437-455.
8. DAI, X. and RAY, A. Damage-mitigating control of a reusable rocket engine: Parts I and II, ASME *J Dynamic Systems, Measurement and Control*, **118**, (3), pp 401-415.
9. HOLMES, M. and RAY, A. Fuzzy damage mitigating control of mechanical structures, *ASME J Dynamic Systems, Measurement and Control*, 1998, **120**, (2), pp 249-256.
10. ROZAK, J.H. and RAY, A. Robust multivariable control of rotorcraft in forward flight, *J Amer Heli Soc*, 1997, **42**, (2), pp 149-160.
11. KALLAPPA, P.T., HOLMES, M. and RAY, A. Life extending control of fossil power plants for structural durability and high performance, *Automatica*, 1997, **33**, (6), pp 1101-1118.
12. KALLAPPA, P.T. and RAY, A. Fuzzy wide range control of fossil power plants for life extension and robust performance, *Automatica*, 2000, **36**, (1), pp 69-82.
13. ZHANG, H. and RAY, A. Robust damage damage-mitigating control of mechanical structures: experimental validation on a test apparatus, *ASME J Dynamic Systems, Measurement and Control*, 1999, **121**, (3), pp 377-385.
14. BUFFINGTON, J.M., SPARKS, A.G. and BANDA, S.S. Robust longitudinal axis flight control for an aircraft with thrust vectoring, *Automatica*, 1994, **30**, (10), pp 1527-1540.
15. DURHAM, W.C. Constrained control allocation, Proceedings of the 1992 AIAA Guidance, Navigation, and Control Conference,1992, pp 1147-1155.
16. ROZAK, J.H. and RAY, A. Robust multivariable control of rotorcraft in forward flight: impact of bandwidth on fatigue life, *J Amer Heli Soc*, 1998, **43**, (3), pp 195-201.
17. BRUMBAUGH, R.W. An aircraft model for the AIAA controls design challenge, AIAA Paper 91-2631, 1991.
18. ADAMS, J.R., BUFFINGTON, J.M., SPARKS, A.G. and BANDA, S.S. *Robust Multivariable Flight Control*, 1994, Springer-Verlag, London.
19. DoD, 1980, Military Specifications — Flying Qualities of Piloted Airplanes, MIL-F-8785C, Department of Defense, Washington, DC.
20. US Standard Atmosphere, 1962, US Government Printing Office, Washington, DC.
21. ETKIN, B. *Dynamics of Atmospheric Flight*, 1972, John Wiley & Sons, New York.
22. CAPLIN, J. Damage-mitigating control of aircraft for high performance and life extension, Doctoral Dissertation in Mechanical Engineering, 1998, Pennsylvania State University, University Park, PA.
23. DOWELL, E.H. (Ed), CRAWLEY, E.F., CURTISS, H.C., PETERS, D.A., SCANLAN, R.H. and SISTO, F. *A Modern Course in Aeroelasticity*, 3rd Ed, 1995, Kluwer Press, Dordrecht, The Netherlands.
24. ALBANO, E. and RODDEN, W.P. A doublet-lattice method for calculating lift distributions on oscillating surfaces in subsonic flows, *AIAA J*, 1969, **7**, (2), pp 279-285; also Errata, **7**, (11), pp 2,192.
25. KARPEL, M. Time-domain aeroservoelastic modelling using weighted unsteady aerodynamic forces, *J Guidance, Control, and Dynamics*, 1990, **13**, (1), pp 30-37.
26. SCHIJVE, J. Observations on the prediction of fatigue crack growth propagation under variable-amplitude loading, fatigue crack growth under spectrum loads, *ASTM STP 595*, 1976, pp 3-23.
27. MCMILLAN, J. C. and PELLOUX, R.M.N. Fatigue crack propagation under program and random loads, fatigue crack propagation, *ASTM STP 415*, 1967, pp 505-532 (Also BSRL Document D1-82-0558, 1966).
28. PORTER, T.R. Method of analysis and prediction for variable amplitude fatigue crack growth, *Eng Fracture Mechanics*, 1972, **4**, pp 717-736.
29. SURESH, S. *Fatigue of Materials*, 1991, Cambridge University Press, Cambridge, UK.
30. NEWMAN, J.C. A crack-closure model for predicting fatigue crack growth under aircraft loading, methods and models for predicting fatigue crack growth under random loading, *ASTM STP* 748, 1981, pp 53-84.
31. NEWMAN, J.C. FASTRAN-II — A fatigue crack growth structural analysis program, NASA Technical Memorandum 104159, 1992, Langley Research Centre, Hampton, VA.
32. NEWMAN., J.C. A crack opening stress equation for fatigue crack growth, *Int J of Fracture*, 1984, 24, pp R131-R135.
33. IBRAHIM, F. K., THOMPSON, J. C. and TOPPER, T. H. A study of effect of mechanical variables on fatigue crack closure and propagation, *Int J of Fatigue*, 1986, **8**, (3), pp 135-142.
34. LORENZO, C.F., HOLMES, M. and RAY, A. Nonlinear life extending control of a rocket engine, *AIAA J of Guidance, Control, and Dynamics*, **23**, (4), pp 759-762.
35. ZHOU, K., DOYLE, J.C. and GLOVER, K. *Robust and Optimal Control*, 1996, Prentice-Hall, NJ.
36. BALAS, G.J., DOYLE, J.C., GLOVER, K., PACKARD, A. and SMITH, R. *μ-Analysis and Synthesis Toolbox*, 1993, MUSYN and The Math Works.
37. BAMIEH, B.A. and PEARSON, J.B. A general framework for linear periodic systems with applications to H_∞–sampled data control, *IEEE Trans on Automatic Control*, 1992, **37**, (4), pp 418-435.
38. SHIVASHANKAR, N. and KHARGONEKAR, P.P. Robust stability and performance analysis of sampled-data systems, *IEEE Trans on Automatic Control*, 1993, 38, (1), pp 58-69.
39. PATANKAR, R. and RAY, A. Damage mitigating controller design for structural durability, *IEEE Trans on Control Systems Technology*, 1999, **7**, (5), pp 606-612.
40. ZHANG, H., RAY, A. and PATANKAR, R. Damage-mitigating control with overload injection: experimental validation of the concept, *ASME J Dynamic Systems, Measurement, and Control*, 2000, **122**, (2), pp 336-342.